Three-Dimensional Fracture Analysis of UIC 60 Rail Failures Using FCPAS

Mürsel Derya, Hakan Dündar and *Ali O. Ayhan
Sakarya University, Faculty of Engineering, Mechanical Engineering Department
54187, Serdivan, Sakarya, TURKEY

Abstract

In this study, three-dimensional fracture analyses are performed for some crack configurations contained in UIC 60 rails, which is one of the most commonly used rail types in Europe. For the fracture analyses, three-dimensional finite element models, which contain specially-formulated enriched crack tip elements, are used. The fracture analyses are performed for two different crack configurations, which represent the crack sizes and shapes under a four-point bending fatigue test at failure. The results show good agreement with fracture results from the literature. Thus, it is concluded that the method used in this study allows accurate representation of three-dimensional fracture conditions for cracks observed in rails.

Key words: Fracture, UIC 60 Rail, Finite Element Method.

1. Introduction

There are many components in railway transportation that undergoes repeated cyclic loads and therefore are prone to fatigue failure. Two of these components that work together under fatigue loads are the train wheel and the rail, and fatigue cracking can be observed on both components during service life. In Ref. [1], Kumar presents main failure modes for rails. These failures are; shelling, head checks, spalling, squats, Tache Ovale, plastic flow and tongue lipping, bolt hole crack, longitudinal vertical crack, transverse crack, buckling and corrugation [1]. From a reliability perspective and for safety of lives, assessment of fracture conditions and damage tolerance for rails is of great importance.

There are studies in the literature that deal with the rail cracks experimentally and numerically. Some of these studies can be summarized as follows: Schöne and Bork [2] performed fatigue tests to monitor propagation of lateral head cracks in UIC 60 rail under three-point bending test conditions and developed empirical crack growth equations. They concluded that the head cracks propagate according to linear elastic fracture mechanics. Schnitzer and Edel [3] analyzed rolling contact-induced fatigue cracks in rails and concluded that the cold working of the rail steel is essential for crack growth. Hassani and Ravaee [4] studied transverse cracks and crack growth in rails both experimentally and numerically. In Ref. [5], Kotsikos and Grasso performed experiments and analyses for web corner cracks and foot base cracks in UIC 60 rails under four-point bending conditions. They performed fatigue experiments until failure, analyzed fracture surfaces and performed finite element analyses of crack configurations at failure to obtain stress

*Corresponding author: Address: Sakarya University, Faculty of Engineering, Department of Mechanical Engineering, 54187, Sakarya TURKEY. E-mail address: ayhan@sakarya.edu.tr, Phone: +90 (264) 295 5656 Fax: +90 (264) 295 5601.

intensity factor distributions. They also performed crack growth simulations for the web corner crack in the rail.

In this study, FCPAS (**F**racture and **C**rack **P**ropagation **A**nalysis **S**ystem) was applied to three-dimensional rail crack problems encountered in practice. Specifically, two surface cracks on the web corner are analyzed and stress intensity factors computed and compared with those of Ref. [5]. This allows the application and validation of FCPAS and its main solver FRAC3D in rail transport cracking problems from the perspective of computation of stress intensity factors for three-dimensional cracks in this practical area. Future studies may include simulation of crack propagation for different types of cracks in rails.

2. Materials and Method

The main and most important method used within FCPAS is the three-dimensional enriched finite element technique incorporated within the solver part of FCPAS, FRAC3D. Other modules of FCPAS either carry out pre-or post-processing related tasks involved in a finite element analysis. In the next subsection, basic details of the enriched element formulation are presented.

2.1. Three-Dimensional Enriched Finite Element Formulation

In Fig. 1, 20-noded hexahedral and 10-noded tetrahedral enriched crack tip elements having an edge or a point on an arbitrarily oriented crack front are shown. It should be noted that the crack front is fully surrounded by these types of elements with edge or point-touches to the crack front. For an integration point at ξ, η and ρ local coordinates in the enriched element, the displacements are given by,

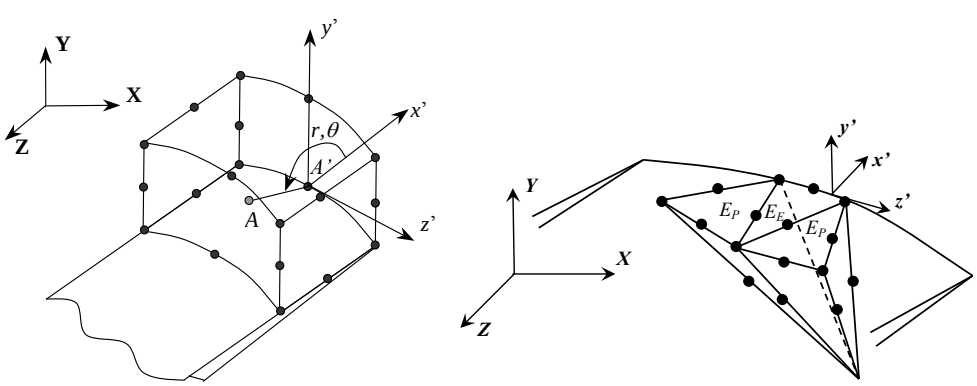

Figure 1: Enriched crack tip elements on an arbitrarily oriented crack front, (a) 20-noded, (b) 10-noded element**.**

$$
\begin{aligned}
u(\xi,\eta,\rho) = \sum_{j=1}^{m} N_j(\xi,\eta,\rho)u_j &+ Z_0(\xi,\eta,\rho)\left(f_u(\xi,\eta,\rho) - \sum_{j=1}^{m} N_j(\xi,\eta,\rho) f_{uj} \right)\left(\sum_{i=1}^{ntip} N_i(\Gamma)K_I^i \right) \\
&+ Z_0(\xi,\eta,\rho)\left(g_u(\xi,\eta,\rho) - \sum_{j=1}^{m} N_j(\xi,\eta,\rho) g_{uj} \right)\left(\sum_{i=1}^{ntip} N_i(\Gamma)K_{II}^i \right) \\
&+ Z_0(\xi,\eta,\rho)\left(h_u(\xi,\eta,\rho) - \sum_{j=1}^{m} N_j(\xi,\eta,\rho) h_{uj} \right)\left(\sum_{i=1}^{ntip} N_i(\Gamma)K_{III}^i \right)
\end{aligned} \tag{1}
$$

$$
\begin{aligned}
v(\xi,\eta,\rho) = \sum_{j=1}^{m} N_j(\xi,\eta,\rho)v_j &+ Z_0(\xi,\eta,\rho)\left(f_v(\xi,\eta,\rho) - \sum_{j=1}^{m} N_j(\xi,\eta,\rho) f_{vj} \right)\left(\sum_{i=1}^{ntip} N_i(\Gamma)K_I^i \right) \\
&+ Z_0(\xi,\eta,\rho)\left(g_v(\xi,\eta,\rho) - \sum_{j=1}^{m} N_j(\xi,\eta,\rho) g_{vj} \right)\left(\sum_{i=1}^{ntip} N_i(\Gamma)K_{II}^i \right) \\
&+ Z_0(\xi,\eta,\rho)\left(h_v(\xi,\eta,\rho) - \sum_{j=1}^{m} N_j(\xi,\eta,\rho) h_{vj} \right)\left(\sum_{i=1}^{ntip} N_i(\Gamma)K_{III}^i \right)
\end{aligned} \tag{2}
$$

$$
\begin{aligned}
w(\xi,\eta,\rho) = \sum_{j=1}^{m} N_j(\xi,\eta,\rho)w_j &+ Z_0(\xi,\eta,\rho)\left(f_w(\xi,\eta,\rho) - \sum_{j=1}^{m} N_j(\xi,\eta,\rho) f_{wj} \right)\left(\sum_{i=1}^{ntip} N_i(\Gamma)K_I^i \right) \\
&+ Z_0(\xi,\eta,\rho)\left(g_w(\xi,\eta,\rho) - \sum_{j=1}^{m} N_j(\xi,\eta,\rho) g_{wj} \right)\left(\sum_{i=1}^{ntip} N_i(\Gamma)K_{II}^i \right) \\
&+ Z_0(\xi,\eta,\rho)\left(h_w(\xi,\eta,\rho) - \sum_{j=1}^{m} N_j(\xi,\eta,\rho) h_{wj} \right)\left(\sum_{i=1}^{ntip} N_i(\Gamma)K_{III}^i \right)
\end{aligned} \tag{3}
$$

In (1)-(3), N_j are the regular finite element shape functions, u_j, v_j and w_j are the nodal displacements, Z_0 is a zeroing function that varies between 0 and 1, m=20 or 10 depending on element type, and f_u, g_u, h_u, f_v, g_v, h_v, f_w, g_w and h_w are obtained from the analytically known functions in the asymptotic crack tip displacement expression and represent the mode I, mode II and mode III displacement components transformed from local (primed axes in Fig. 2) to the global coordinate system. For the evaluation of asymptotic crack field terms, given an integration point within an enriched element, the corresponding perpendicularly intersected crack front position is determined. Since the three-dimensional crack fields are identical to those of plane strain conditions when evaluated within the planes perpendicular to the crack front, the corresponding local coordinate system is positioned such that the local (primed) *x-y* plane is perpendicular and local *z* axis is tangential to the crack front (Fig. 2). K_I^i, K_{II}^i and K_{III}^i in (1)-(3) are the unknown nodal stress intensity factors for the crack front nodes within the element and the neighboring nodes on the crack front. Therefore, the term $\left(\sum_{i=1}^{ntip} N_i(\Gamma)K_{I,II,III}^i \right)$ describes the variation of the stress intensity factors along the whole crack front in a piecewise fashion, in which *ntip* is 3 for the quadratic enriched element. The local isoparametric coordinate Γ varies between -1 and 1.

Computation of stiffness matrices of enriched elements includes derivatives of the above displacement fields. These derivatives for a quadratic tetrahedral enriched element and details related to integration and transition elements are given in Ref. [6]. Once the element stiffness matrices for all elements in the model are computed, they are included in the solution phase to

obtain the nodal displacements and stress intensity factors on the crack front nodes without any post-processing efforts.

2.2. The Finite Element Fracture Models

The models used in this study represent four-point bending tests performed in [5] on a UIC 60 rail. The geometric and loading details in their study are as follows: The distance between the supports and the loading point span are, respectively, 750 mm and 190 mm. The finite element fracture models used in this study are generated using ANSYS^{TM} [7] and are solved within FCPAS to compute stress intensity factors for the chosen crack configurations at rail failure from Ref. [5]. First, a stress analysis is performed for the four-bending test without a crack to show the higher bending stresses on the rail base (foot) and the web corner (Fig. 2). As can be seen from this figure, the symmetry in the axial direction of the rail is taken into account by modeling half of the geometry.

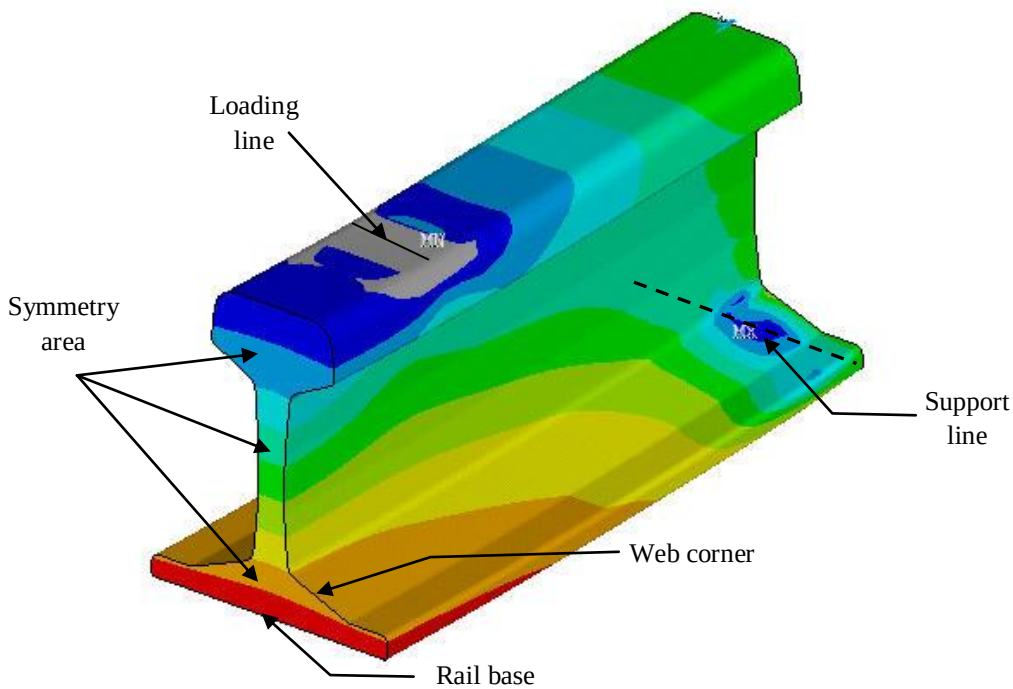

Figure 2: Distribution of bending stresses under four-point bending conditions – no crack.

Next, the finite element fracture models for the two crack configurations at failure during the four-point bending test are developed. Fig. 3 shows the first crack configuration assessed in [5].

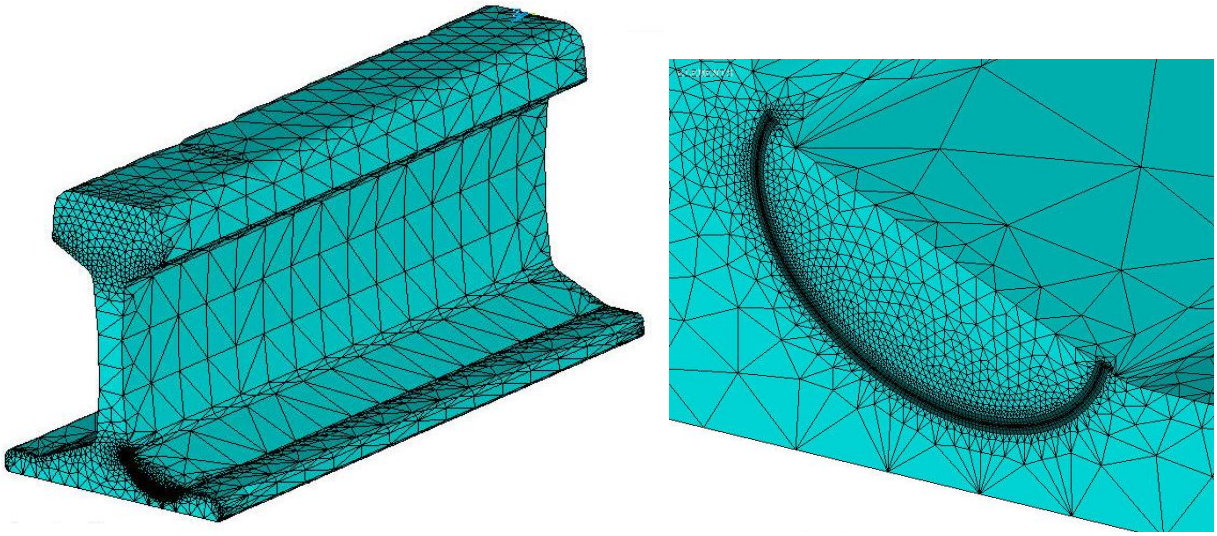

(a) **(b)**

Figure 3: Finite element fracture model for UIC 60 crack #1, **(a)** Global view, **(b)** Close-up view of crack region.

Similar to the stress analysis model, symmetry in the axial direction is taken into account by imposing appropriate boundary conditions. It is seen from Fig. 3 that near the crack front hexahedral elements are used to better capture the highly varying stress state in this region, whereas tetrahedral elements are used everywhere else in the model. The hexahedral elements that have borders with the crack front are the enriched elements that contain the stress intensity factors in their formulation. Similarly, Fig. 4 shows the finite element fracture model for the third crack configuration studied in Ref. [5].

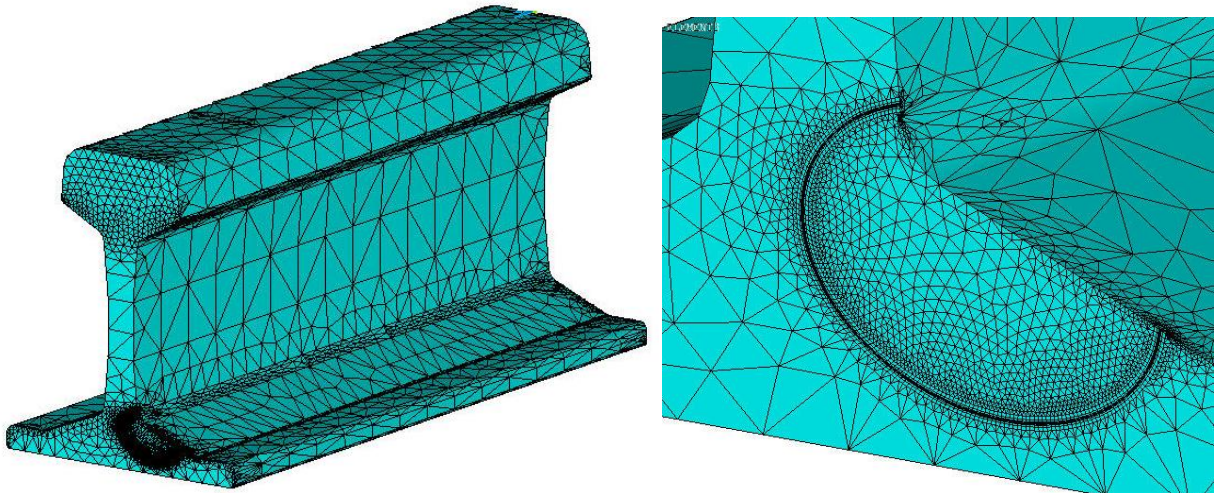

(a) **(b)**

Figure 4: Finite element fracture model for UIC 60 crack #3, **(a)** Global view, **(b)** Close-up view of crack region.

3. Results

In this section, results from fracture analyses are presented for the two crack configurations presented above in terms of stress intensity factor distributions along the crack fronts.

3.1. Fracture Analysis Results

In Fig. 5 and Fig. 6, mode-I stress intensity factor distributions are presented for the two crack configurations under a maximum failure load of 582 kN as described in [5]. These solutions obtained using three-dimensional enriched finite elements agree reasonably well with those of [5]. It is stated in their study that the critical stress intensity factor for the rail material is K_Q=27 ± 2 MN-m$^{-3/2}$. Thus, it is clear from both figures that in some portion of the crack front under the stated load, the stress intensity factors are above the critical failure, and thus imply fracture failure as observed by experiments done in [5].

Figs. 7 and 8 show the bending stress contours for the two fracture models, namely crack#1 and crack#3. It is seen from both figures that the stresses along the crack front are, as expected, much higher than the bending stresses away from the crack.

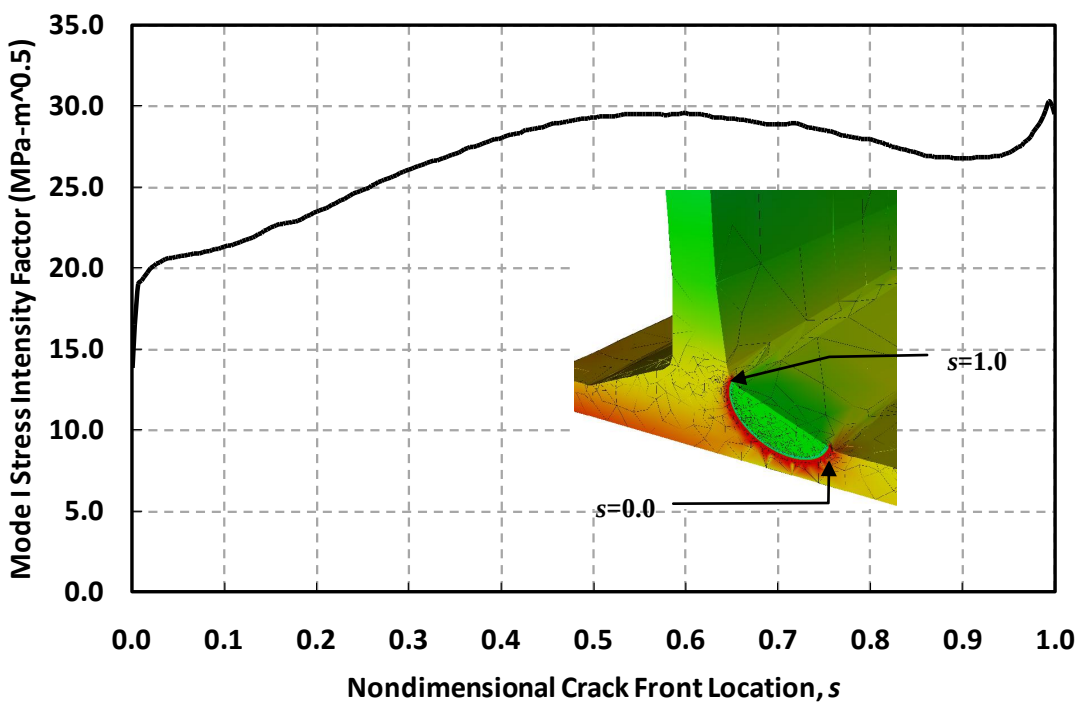

Figure 5: Mode-I stress intensity factor distribution along crack front for UIC 60 rail, crack #1.

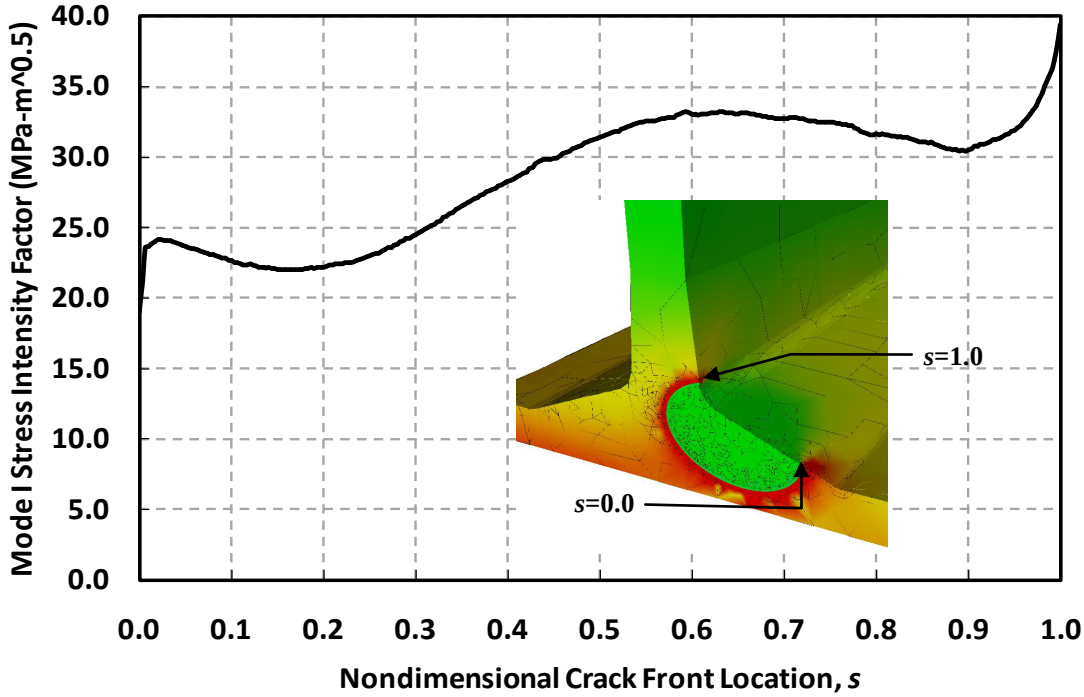

Figure 6: Mode-I stress intensity factor distribution along crack front for UIC 60 rail, crack #3.

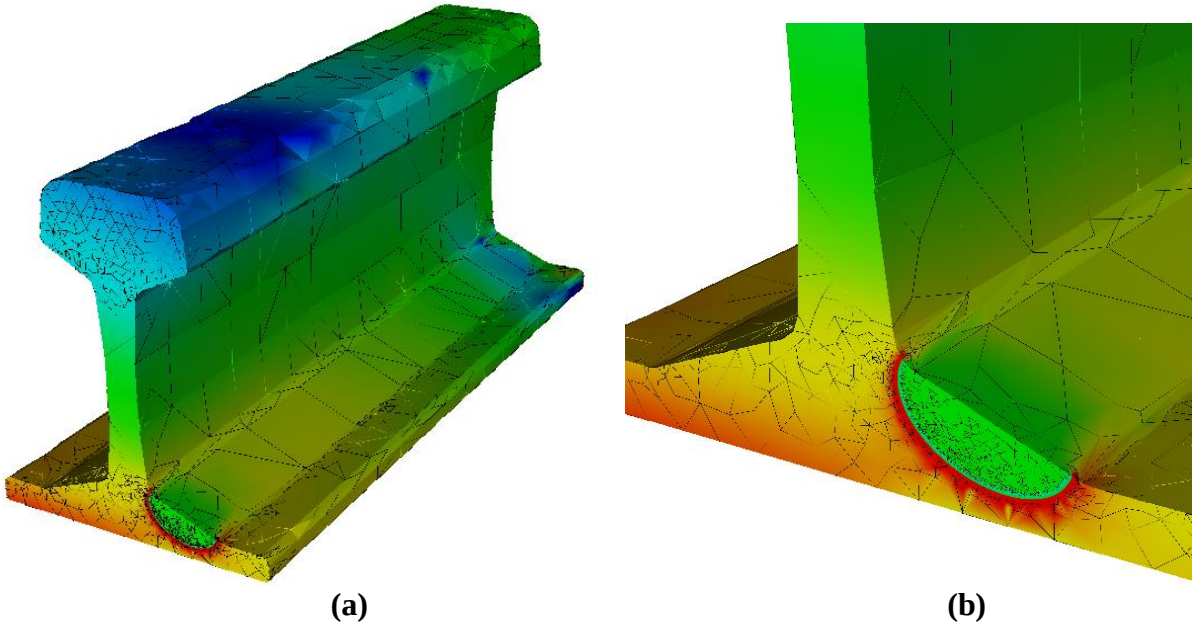

Figure 7: Bending stresses for UIC 60 rail, crack #1, **(a)** Global view, **(b)** Close-up view of crack region.

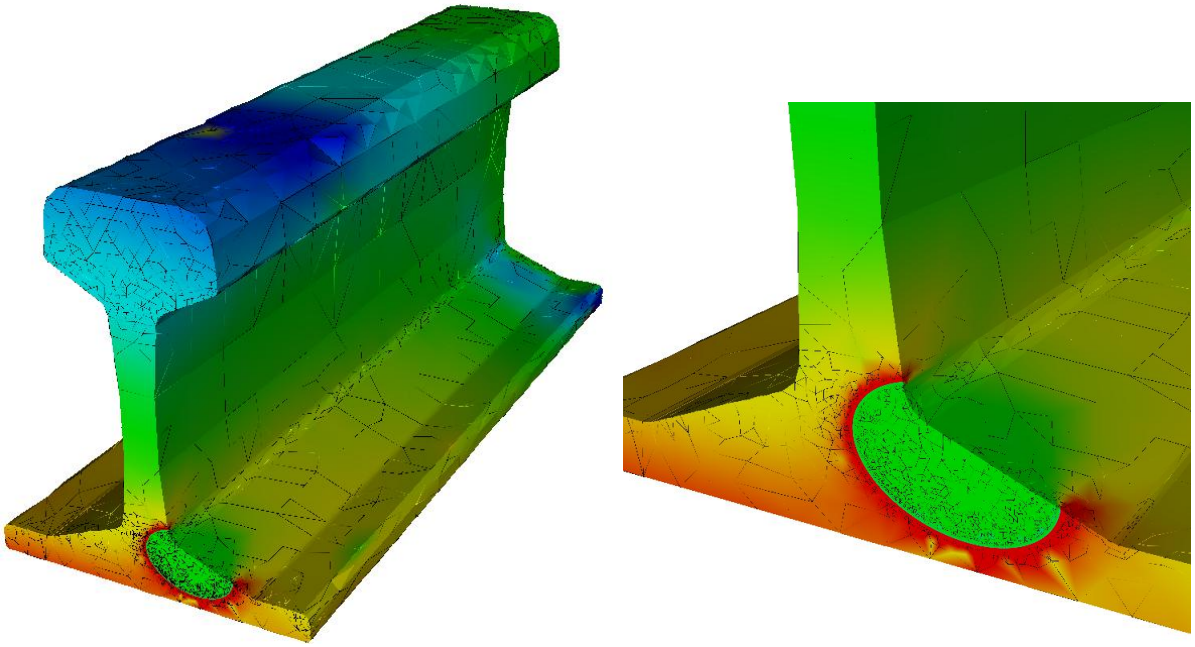

(a) **(b)**

Figure 8: Bending stresses for UIC 60 rail, crack #3, **(a)** Global view, **(b)** Close-up view of crack region.

4. Discussion

In the absence of any specialized procedure and tools, preparation of three-dimensional fracture models are mostly time consuming and require extensive effort and care. This is because, in most fracture analysis software, special meshes are needed along the crack front to simulate the high stress and strain gradients. On the other hand, the method applied in this study, namely three-dimensional enriched elements, have special element formulations that incorporate stress intensity factors as unknowns and don't require special meshes and post processing of results. As seen from the above results for UIC 60 rail cracks, the three-dimensional enriched finite elements used in this study produce fracture results that are accurate and represent the real conditions seen in the experimental work in the literature.

The results presented in this study are based on two discrete crack configurations that were assigned as failure crack size and shapes in [5]. Future studies on this subject can be done by performing crack propagation analyses for a variety of crack types in rails including, web corner, base and head cracks using the existing mode-I crack propagation capability within FCPAS. There are benefits of being able to simulate crack propagation and remaining life assessment for rail cracks. Once a crack of certain size and shape is detected on rails by NDE inspectors, predicting its remaining life with some factor of safety can help reduce any catastrophic failures and accidents in rail transportation and eliminate unnecessary early replacements.

Conclusions

The **F**racture and **C**rack **P**ropagation **A**nalysis **S**ystem (FCPAS) was applied in this study to UIC 60 rail web corner cracks. The aim in this study was to validate the usage of FCPAS in some rail transport applications. Two different three-dimensional surface crack cases, i.e., different size and shapes, are analyzed under the conditions of four-point bending test for which experimental and numerical results are available in the literature. The stress intensity factor distributions obtained in this study showed reasonably good agreement with those existing in the literature. It was also seen that the stress intensity factors go slightly above its critical value for the rail material along some portions of the crack fronts, and thus, are indicative of the real failures seen in the experimental study in the literature. Therefore, it is concluded that having applied and validated the stress intensity factor computation, crack propagation and fatigue life calculations can be performed as part of future studies on this subject.

Acknowledgements

This study is performed as a new application of FCPAS to some problems in rail transportation area and to compare its results those existing in the literature. Initial rail model geometry development and exploratory fracture analyses of circular cracks performed by the graduating senior students, M. Bozkurt, S. C. Eras and S. Çanlı, are acknowledged.

References

[1] Kumar, S. Study of Rail Breaks: Associated Risks and Maintenance Strategies. Technical Report. http://epubl.ltu.se/1402-1536/2006/07/LTU-TR-0607-SE.pdf. 2006.

[2] Schöne, D., Bork, C. P. Fatigue Investigations of Dameged Railway Rails of UIC 60 Profile. Proceedings of ECF18, Dresden, Germany, October 14, 2012. http://www.gruppofrattura.it/ocs/index.php/esis/ECF18/paper/viewFile/6139/2015

[3] Schnitzer, T., Edel, K.-O. Fracture Mechanical Analysis and Assessment of The Extension of Rolling Contact Fatigue Cracks in Railway Rails. 7th International Conference on Contact Mechanics and Wear of Rail/Wheel Systems (CM2006), Brisbane, Australia; September 24-26, 2006, p. 473-479.

[4] Hassani, A., Ravaee, R. Characterization of Transverse Crack and Crack Growth in a Railway Rail. Iranian Journal of Materials Science and Engineering 2008;5-2: 22-31.

[5] Kotsikos, G., Grasso, M. Assessment of Fatigue Cracks in Rails. Procedia Social and Behavioral Sciences, Transport Research Arena – Europe 2012; 48: 1395-1402.

[6] Ayhan, A.O., Nied, H.F. Stress intensity factors for three-dimensional surface cracks using enriched finite elements. International Journal for Numerical Methods in Engineering; 2002; 54:899–921.

[7] ANSYS, Version 12.0, Ansys Inc., Canonsburg, PA, USA, 2009.